A

B

Figure S1 Resection at the I-Sce-I array. (**A**) Immmunofluorescence microscopy on NIH-2/4 cells transiently transfected with CFP lacR and RFP-I-SceI-GR in the presence of TA. Cells were stained with the indicated antibody.Scale bar 5μm. (**B**) Recruitment kinetics of RPA after addition of TA. Values represent the percentage of positive cells (n= 100). The error bars represent the standard deviation of 3 independent data sets.
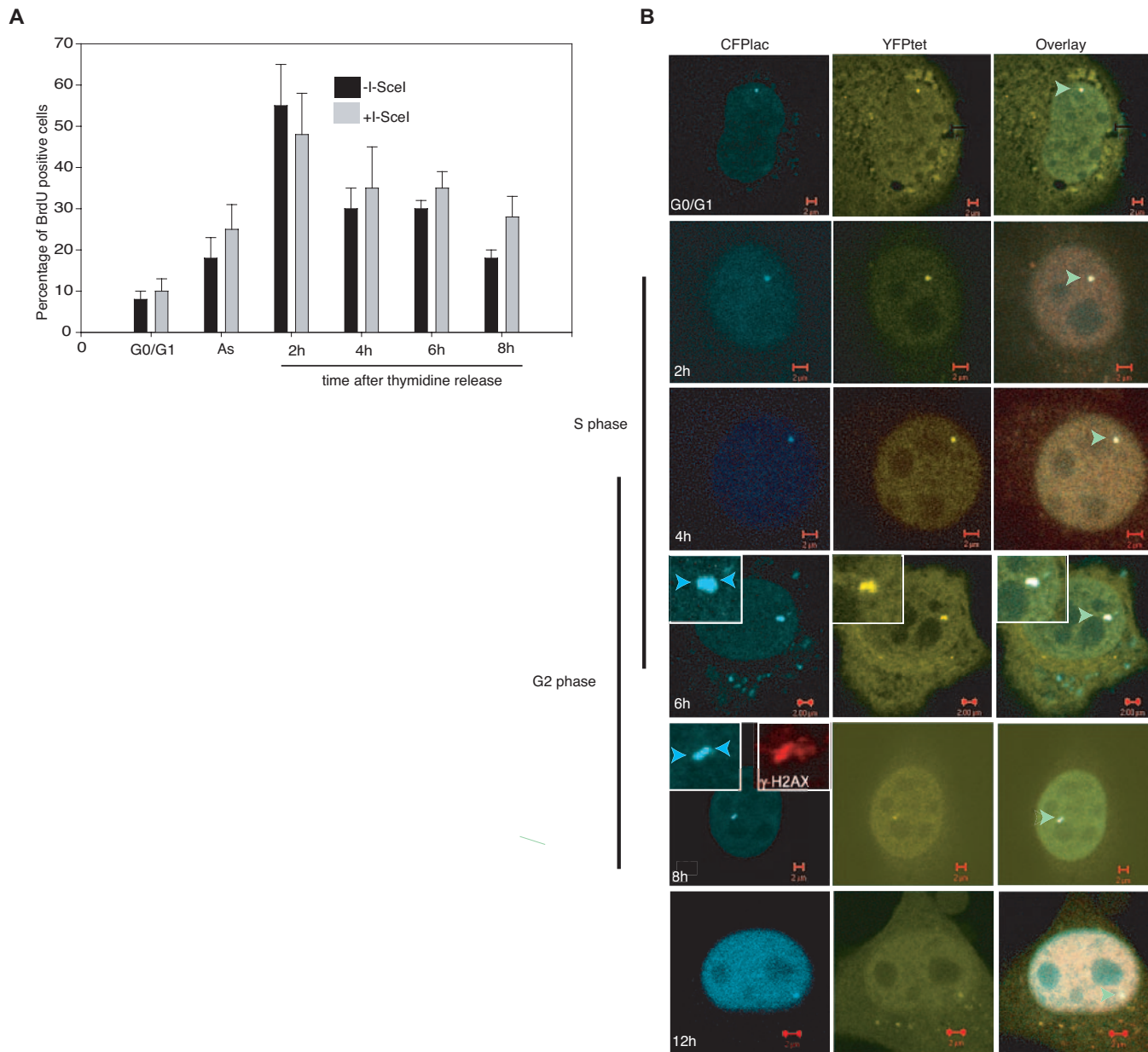
A

B

Figure S2 Analysis of the positional stability of broken DNA ends during the cell cycle. **(A)** Quantification of S-phase progression of control cells or cells expressing RFP-I-SceI-GR arrested in G0/G1 or after release from a G1/S boundary arrest by double thymidine block. **(B)** Confocal images and quantification of CFP and YFP tag colocalization in NIH2/4 cells arrested in G0/G1 or at indicated time points after double thymidine block and release into S-G2 phase. No separation of the broken ends was observed at any time point indicating that the constrained motion of DSBs is not cell cycle specific. Scale bar 2μm. Note that in G2 we frequently observe two spots for the array and γ-H2AX staining covers the two typically in a continuous spot (insets).
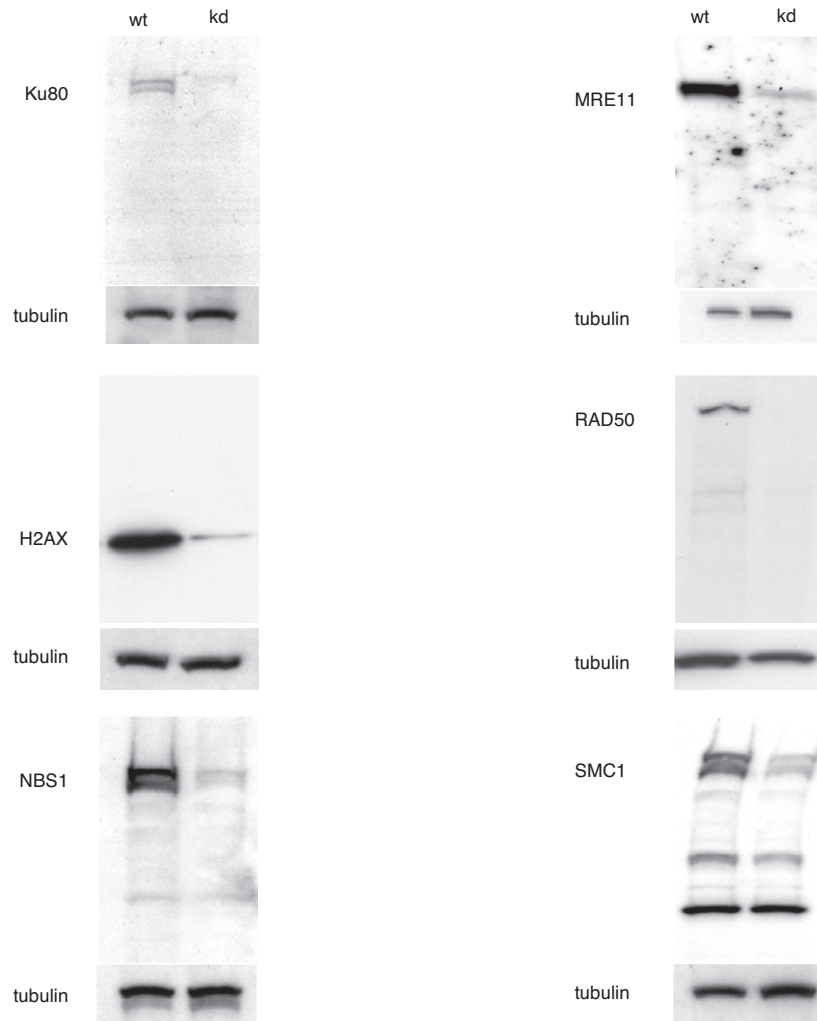
Figure S3 Efficiency of depletion of DNA repair factors by RNAi. Western blot analysis of control NIH 2/4 cells and cells subjected to two sequential transfections with siRNAs (100nM) against the indicated proteins and analyzed 48 hours after the first delivery. Alpha-tubulin immunoblotting was used as a loading control.
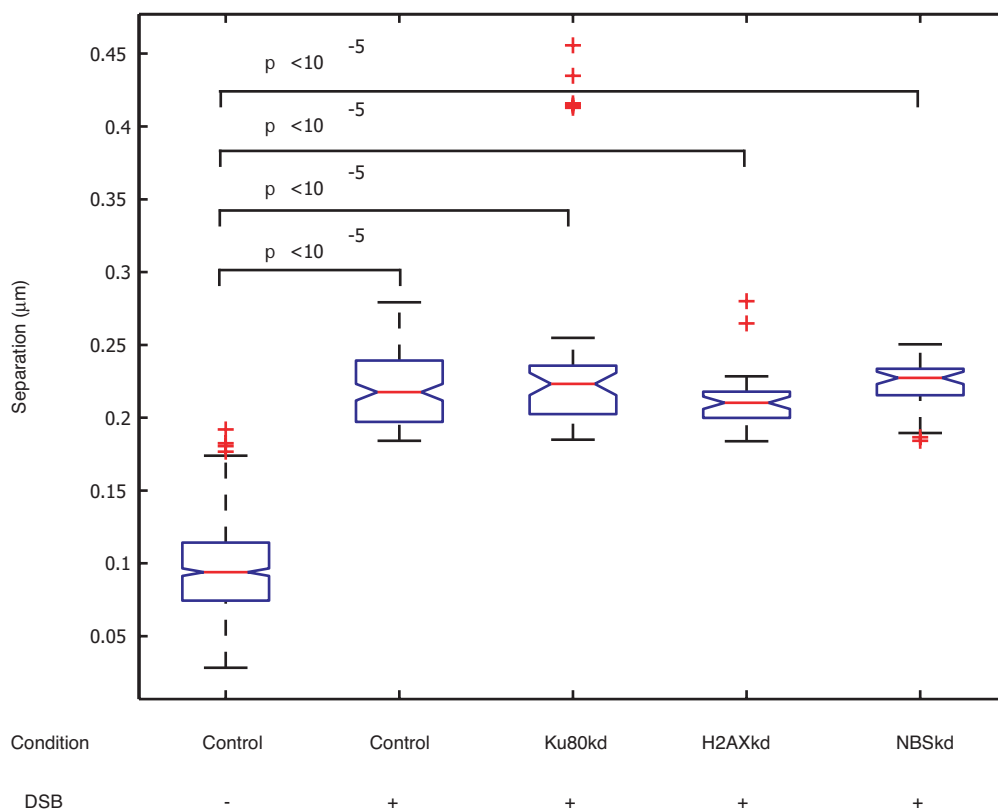
Figure S4 Analysis of the local movement of broken DNA ends. Distribution of tag separation in control and Ku80, H2AX and NBS1 depleted cells. With DSB, separation increases from ~0.1 μm to ~0.22 μm ($p<10^{-5}$) in all cases. Boxes indicate boundaries of the 25th percentile to the 75th percentile. The red line indicates the median of the data. Error bars indicate the spread of the data. Outliers are marked by red crosses, and are defined as data points that further than 1.5 times the size of the box. . P values were obtained by t-test and represent pairwise comparisons of the indicated sample means.
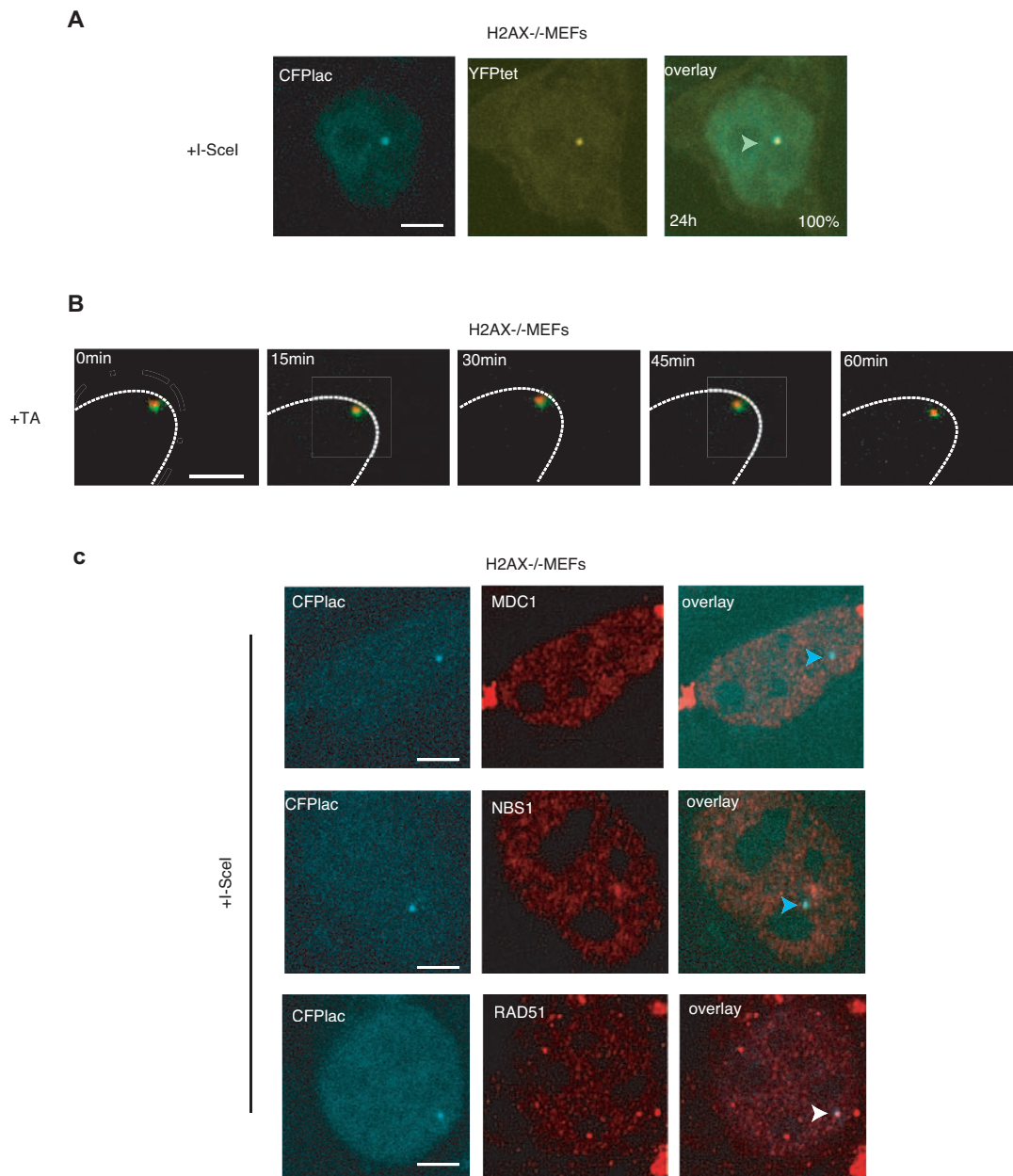
A

H2AX-/-MEFs

B

H2AX-/-MEFs

C

H2AX-/-MEFs

Figure S5 Analysis of positional and local movement of broken ends in H2AX-/- MEFs. **(A)** Confocal images and quantification of CFP and YFP tag colocalization in H2AX-/- cells 24 hours after induction of a DSB by I-SceI expression. No separation of tags was detected (N=50). **(B)** Representative time points of a time-lapse series 60 min after the addition of TA in H2AX-/- cell containing a single array. Each time point is a color combined maximum projection of 3D stacks recorded in CFP (red) and YFP (green) channels.

(C) Indirect immmunofluorescence on H2AX-/- cells containing a Lac-I-SceI-tet array transfected with CFP lacR and HA-I-SceI plasmids. Cells were stained with the indicated antibodies. No accumulation of MDC1 and NBS1 was detected on the array containing a DSB. Accumulation of RAD51 was observed in a subpopulation of cells confirming efficient cutting at the I-SceI site in H2AX -/- cells.

SUPPLEMETARY MATERIALS

Methods

Plasmids

To generate the lac-I-SceI-tet plasmid we subcloned the 256 lac operator repeats (XhoI fragment) and the 96 tet operator repeats (XhoI –SacII fragment) from the p16PCbeta plasmid (gift from D. Spector [1]) into pBluescript. Between the two fragments a single 18nt I-SceI site was inserted (SalI). The CFPlacR and YFP tet R expression vector plasmids were gifts from D. Spector. For the binding of YFP tet repressor to the corresponding array, Doxycyclin (Clontech) was added in the medium in a final concentration 1μ/ml. To generate the I-SceI-GRLBD construct, the Ligand Binding Domain (LBD) of GR was amplified from pCI-nGFP-C656G GR (gift from G. Hager [2]) with the primers 5'CGGTACCGCGGGTATCGGAAATGTCTT3' and 5'CCCGGGATCCATTTTTGATGAAACAGAAG3' and cloned into pEGFP-C2 (Clontech) in the SacII and BamHI sites. Similarly, the I-SceI cDNA was amplified from the HA-I-SceI [3] using the primers 5'GATCTCGAGCTCAATGAAAAACATCAA3' and 5'TGAAGTCGACATTTCAGGAAAGTTTC3' and cloned into the previously described GFP-GRLBD into the SacI and SalI restriction sites. Finally, the chimeric I-SceI –GR cDNA was subcloned into pmRFP (Clontech) into the SacI and BamH I sites using the following primers: 5'GGAAGAGCTCAAATGAAAAACATCAA3' and 5'CCCGGGATCCATTTTTGATGAAACAGAAG3'

Western blotting

Cells subjected to 2 rounds of transfection using a specific siRNA were collected 2 days after the first transfection, washed in PBS and resuspended in Laemmli buffer. Equal amounts of the protein samples were loaded on 4%-12%gradient gels (Biorad).Blotting and immunodetection were performed as described [4] using the described antibodies.

SKY analysis and chromosome paint in interphase.

SKY analysis was performed as described [5]. Interphase chromosome paint analysis was performed as described [6]. Briefly, NIH-2/4 cells were plated at 70% confluency on glass cover slips, permeabilized in CSK buffer and fixed in 4% PFA. The fixed cells were subjected to 0.1NHCL and 4-5 freeze-thaw cycles. Coverslips were hybridized for 48 h at

37°C in a moist chamber with a combination of two or three painting probes at a time. Probes were prepared from flow-sorted chromosomes by degenerate oligonucleotide-primed polymerase chain reaction (PCR) as described [7]. Images of double or triple-labeled cell nuclei were generated using the Zeiss LSM META confocal microscope and analyzed using Zeiss LSM Examiner (Zeiss). All measurements were performed on maximum projections of 12 focal planes covering the entire nucleus. Chromosomes in the projections were visually compared to the single focal planes to verify that the regions were representative of the entire chromosome. Proximal positioning was defined as physical association of pixels representing distinct chromosomes as described [6].

Image analysis

3D time-lapse sequences were analyzed with custom-written spot tracking software as described previously [8]. Briefly, 3D Gaussians were automatically fitted onto the intensity distributions of the CFP and YFP tag signals, and statistically tested for significance of the estimated tag amplitudes. Whenever a tag signal was sufficiently deformed to allow the fitting of a second Gaussian into the same intensity distribution, or when the tags moved out of the image, the frame was discarded. The detection algorithm returned for both tags the 3D positions and the positional uncertainty as estimated for every tag and time point [8]. These positions were then corrected for lateral and axial shifts of the CFP and YFP channels associated with chromatic aberration and slight misalignment of excitation and emission filters. The shift between the channels was determined by imaging Cajal bodies jointly labeled with both CFP-coilin and YFP-coilin in HeLa cells with the same microscopy settings as used for time-lapse imaging.

To describe the joint motion of CFP and YFP tags in a rotation and shift-invariant manner, we calculated the CFP-YFP tag distance as the norm of the 3D vector connecting the two adjusted tag positions in every frame with propagation of the positional uncertainties of the tags [9]. Critically, due to anisotropy in resolution and sampling between the lateral and axial directions, the distance uncertainty varies with the spatial orientation of the tag-to-tag vector. Moreover, the signal to noise ratio varied significantly between movies as well as throughout a movie. This heterogeneity in distance uncertainty between data points had to be accounted for in the subsequent analysis of tag disjointness.

To assess whether a DSB had occurred, we calculated a "disjointness probability" p_D by statistically comparing the separation between tags and the relative tag mobility in cells after addition of TA to the distribution of these parameters in control cells. A large p_D indicates that tag separation and relative tag mobility are very different from the control, and that it is therefore likely that a DSB has occurred. Since it was conceivable that the DSB occurred during the observation, we determined p_D locally in every CFP to-YFP tag distance trajectory on 10-frame sliding windows.

We calculated tag separation s_i for each sliding window i as the distance average weighted by the distance uncertainty, and we calculated the relative tag mobility m_i as the average absolute distance change between time points, weighted by the uncertainties of the individual distance changes. We then calculated the disjointness coefficient D_i as the difference of tag separation and relative tag mobility in each window to the average separation and mobility of control cells as

$$D_i = \left(\frac{\max\left(s_i - \mu_s, 0\right)}{\sigma_s} \right)^2 + \left(\frac{1}{\sqrt{2}} \frac{\max\left(m_i - \mu_m, 0\right)}{\sigma_m} \right)^2 \sim \chi^2_{2,\infty}$$

(1)

where μ_s and σ_s sigmas are mean and standard deviation over all individual tag separation measurements s_i in control cells, and where μ_m and σ_m are mean and standard deviation over all individual relative tag mobility measurements m_i in control cells. Since the relative tag mobility is calculated as the first difference of a noisy signal, its fluctuations will artificially increase by $\sqrt{2}$, which we compensated for. Furthermore, since a large disjointness coefficient is only of interest to us if separation and mobility strongly increase compared to the control, we set s_i to μ_s and m_i to μ_m if they were below the respective averages.

Equation (1) describes a Mahanalobis distance [10], which follows a χ^2 with two degrees of freedom, which we used to transform the disjointness coefficient D into the disjointness probability p_D. We considered the DNA to be intact if the disjointness probability was below 75%, while a disjointness probability above 95% was considered indicative of a DSB.

Because it was possible that there was leakage of the restriction enzyme into the nucleus in the absence of TA leading to a DSB in control cells, we determined μ_s, σ_s, μ_m, and

σ_m in an iterative process: First, we determined p_D for all 22 -TA trajectories. Then we removed the three trajectories which showed p_D above 75%, and recalculated the four parameters that describe the distribution of separation and mobility in control cells without DSBs.

Separation and mobility of trajectory regions with or without DSB were compared to control using both the parametric two-sided *t*-test with correction for unequal variance, and the non-parametric ranksum test [10]. For all tests, p-values were in good agreement. In the manuscript, the p-values obtained with the *t*-test are given.

References

1. Tsukamoto, T. et al. Visualization of gene activity in living cells. *Nat Cell Biol* **2**, 871-8 (2000).

2. Htun, H., Barsony, J., Renyi, I., Gould, D. L. & Hager, G. L. Visualization of glucocorticoid receptor translocation and intranuclear organization in living cells with a green fluorescent protein chimera. *Proc Natl Acad Sci U S A* **93**, 4845-50 (1996).

3. Rouet, P., Smih, F. & Jasin, M. Expression of a site-specific endonuclease stimulates homologous recombination in mammalian cells. *Proc Natl Acad Sci U S A* **91**, 6064-8 (1994).

4. Soutoglou, E. & Talianidis, I. Coordination of PIC assembly and chromatin remodeling during differentiation-induced gene activation. *Science* **295**, 1901-4 (2002).

5. McNeil, N. & Ried, T. Novel molecular cytogenetic techniques for identifying complex chromosomal rearrangements: technology and applications in molecular medicine. *Expert Rev Mol Med* **2000**, 1-14 (2000).

6. Parada, L. A., McQueen, P. G., Munson, P. J. & Misteli, T. Conservation of relative chromosome positioning in normal and cancer cells. *Curr Biol* **12**, 1692-7 (2002).

7.   Liyanage, M. et al. Multicolour spectral karyotyping of mouse chromosomes. *Nat Genet* **14**, 312-5 (1996).

8.   Thomann, D., Dorn, J., Sorger, P. K. & Danuser, G. Automatic fluorescent tag localization II: Improvement in super-resolution by relative tracking. *J Microsc* **211**, 230-48 (2003).

9.   Dorn, J. F. et al. Yeast kinetochore microtubule dynamics analyzed by high-resolution three-dimensional microscopy. *Biophys J* **89**, 2835-54 (2005).

10.   Fugunaga, K. *Introduction to statistical pattern recognition* (ed. 2nd, A. p.) (1990).

SMC1 smart pool:
Duplex 1: sense   5'-GUACAAGGGUCGACAGAUUUU-3'
        antisense 5'-PAAUCUGUCGACCCUUGUACUU-3'
Duplex 2: sense   5'-GAAAGGAGGCCAAACAAGAUU-3'
        antisense 5'-PUCUUGUUUGGCCUCCUUUCUU-3'
Duplex 3: sense   5'-GCAGGCAUUUGAACAGAUAUU-3'
        antisense 5'-PUAUCUGUUCAAAUGCCUGCUU-3'
Duplex 4: sense   5'-GAAAUUGGUGUGCGUAACAUU-3'
        antisense 5'-PUGUUACGCACACCAAUUUCUU-3'

H2AX smart pool:
Duplex 1: sense   5'-GGAAAGGCCACUACGCCGAUU-3'
        antisense 5'-PUCGGCGUAGUGGCCUUUCCUU-3'
Duplex 2: sense   5'-UCGAGUACCUCACUGCCGAUU-3'
        antisense 5'-PUCGGCAGUGAGGUACUCGAUU-3'
Duplex 3: sense   5'-UCAACAAGCUGCUGGGCGGUU-3'
        antisense 5'-PCCGCCCAGCAGCUUGUUGAUU-3'
Duplex 4: sense   5'-CCCAAGAAGAGCAGCGCCAUU-3'
        antisense 5'-PUGGCGCUGCUCUUCUUGGGUU-3'

NBS1 smart pool:
Duplex 1: sense   5'-GGAAACUGCUGCUGACUGAUU-3'
        antisense 5'-PUCAGUCAGCAGCAGUUUCCUU-3'
Duplex 2: sense   5'-GGAUGGAGCUGUCCUGUUCUU-3'
        antisense 5'-PGAACAGGACAGCUCCAUCCUU-3'
Duplex 3: sense   5'-GCAGUUAAAGUCACCAUUAUU-3'
        antisense 5'-PUAAUGGUGACUUUAACUGCUU-3'
Duplex 4: sense   5'-GGAGAACCAUACCGACUUUUU-3'
        antisense 5'-PAAAGUCGGUAUGGUUCUCCUU-3'

Ku80 smart pool:
Duplex 1: sense   5'-GCAAAGAAAGUGAUGACUAUU-3'
        antisense 5'-PUAGUCAUCACUUUCUUUGCUU-3'
Duplex 2: sense   5'-GUUAAUAAGUCACAUCGAAUU-3'
        antisense 5'-PUUCGAUGUGACUUAUUAACUU-3'
Duplex 3: sense   5'-CCUAUGAGCGUUUAGUUUAUU-3'
        antisense 5'-PUAAACUAAACGCUCAUAGGUU-3'
Duplex 4: sense   5'-CCGAUAUGCUUAUGACAAAUU-3'
        antisense 5'-PUUUGUCAUAAGCAUAUCGGUU-3'

MRE11 smart pool:
Duplex 1: sense   5'-GGAUGGCAAUCUCAACAUUUU-3'
        antisense 5'-PAAUGUUGAGAUUGCCAUCCUU-3'
Duplex 2: sense   5'-GCGAAGCAGUUCAAGAGUUUU-3'
        antisense 5'-PAACUCUUGAACUGCUUCGCUU-3'
Duplex 3: sense   5'-UAGAGUAGAAGACCUCGUAUU-3'
        antisense 5'-PUACGAGGUCUUCUACUCUAUU-3'
Duplex 4: sense   5'-UCGAGGAAUUAGUGAAGUAUU-3'
        antisense 5'-PUACUUCACUAAUUCCUCGAUU-3'

RAD50 smart pool:
Duplex 1: sense   5'-GCUCAGAGAUUGUCAAGUGUU-3'
        antisense 5'-PCACUUGACAAUCUCUGAGCUU-3'
Duplex 2: sense   5'-GCGGAAACCUUCUGUCUGAUU-3'
        antisense 5'-PUCAGACAGAAGGUUUCCGCUU-3'
Duplex 3: sense   5'-GGUAAUCACUCACGAUGAAUU-3'
        antisense 5'-PUUCAUCGUGAGUGAUUACCUU-3'
Duplex 4: sense   5'-GAACAAAGAGCUAGCUUCAUU-3'
        antisense 5'-PUGAAGCUAGCUCUUUGUUCUU-3